Effect of Sr substitution on the room temperature electrical properties of $La_{1-x}Sr_xFeO_3$ nano-crystalline materials

Cite as: AIP Conference Proceedings **1862**, 030042 (2017); https://doi.org/10.1063/1.4991146
Published Online: 10 July 2017

C. A. Kafa, D. Triyono, and H. Laysandra

Effect of Sr Substitution on the Room Temperature Electrical Properties of $La_{1-x}Sr_xFeO_3$ Nano-crystalline Materials

C. A. Kafa, D. Triyono[a)], and H. Laysandra

Department of Physics, Faculty of Mathematics and Natural Sciences (FMIPA), Universitas Indonesia, Depok 16424, Indonesia

[a)]Corresponding author: djoko.triyono@sci.ui.ac.id

Abstract. $LaFeO_3$ is a material with Perovskite structure which electrical properties got investigated a lot, because as a p-type semiconductor it showed good gas sensing behavior through resistivity comparison. Sr doping on $LaFeO_3$ is able to improve the electrical conductivity through structural modification. Using the Sr atoms doping concentration (x) from 0.1 to 0.4, $La_{1-x}Sr_xFeO_3$ nanocrystal pellets were synthesized using sol-gel method, followed by gradual heat treatment and uniaxial compaction. Structural analysis from XRD characterization shows that the structure of the materials is Orthorhombic Perovskite. The topography of the sample by SEM reveals grain and grain boundary existence with emerging agglomeration. The electrical properties of the material, as functions of frequency, were measured by Impedance Spectroscopy method using RLC meter. Through the Nyquist plot and Bode plot, the electrical conductivity of $La_{1-x}Sr_xFeO_3$ is contributed by grain and grain boundaries. It is reported that $La_{0.6}Sr_{0.4}FeO_3$ sample has the most superior electrical conductivity of all samples, and the electrical permittivity of both $La_{0.8}Sr_{0.2}FeO_3$ and $La_{0.7}Sr_{0.3}FeO_3$ are the most stable.

INTRODUCTION

$LaFeO_3$ perovskite has been widely known for various researches and developments. Structurally, this compound is an Orthorhombic crystal with space group Pnma, which is a distortion from ideal cubic structure [1]. However, its properties can be enhanced through doping or partial substitution that caused oxygen vacancy δ and/ or valence state alteration [2]. For this purpose, such requirements for the doping are having less oxidation numbers from the forming cations of the crystal, and causing the average grain size of the crystal to decrease.

Sr^{2+} cation is one well-known doping for increasing $LaFeO_3$ electrical conductivity, by generating oxygen vacancies δ that increasing O^{2-} ion mobility, and/ or causing the Fe cation oxidized from Fe^{3+} to Fe^{4+} [3]. The size and oxidation numbers of Sr^{2+} cation doping towards $LaFeO_3$ perovskite would affect its electrocatalytic behavior, however, these values are adjustable by doping composition calculation to achieve the desirable certain degree.

When Sr^{2+} cation is doped into $LaFeO_3$, there are three types of electrical conductivity arise. First is the electronic conductivity from charge carriers indicated by a shift of the valence state Fe cation (Equation 1), second is the ionic conductivity from O^{2-} anion indicated by oxygen vacancy (Equation 2), and third is the mixed conductivity from both (Equation 3) [4].

$$(La^{3+}_{1-x}Sr^{2+}_{x})(Fe^{3+}_{1-x}Fe^{4+}_{x})O_3 \tag{1}$$

$$(La^{3+}_{1-x}Sr^{2+}_{x})Fe^{3+}(O^{2-}_{3-(x/2)}\delta_{(x/2)}) \tag{2}$$

$$(La^{3+}_{1-x}Sr^{2+}_{x})(Fe^{3+}_{1-y}Fe^{4+}_{y})(O^{2-}_{3-((x-y)/2)}\delta_{((x-y)/2)}) \tag{3}$$

International Symposium on Current Progress in Mathematics and Sciences 2016 (ISCPMS 2016)
AIP Conf. Proc. 1862, 030042-1–030042-6; doi: 10.1063/1.4991146
Published by AIP Publishing. 978-0-7354-1536-2/$30.00

In this work, the range of Sr doping on $LaFeO_3$ used is from x = 0.1 to x = 0.4. This is based on previous experiments showing that the Orthorhombic structure was still retained until the composition of $La_{0.6}Sr_{0.4}FeO_3$, if Sr dopant compositions are the multiple of 0.1 [5, 6]. Moreover, this doping limit is also found to have the ideal value of oxygen nonstoichiometry δ that retains good ionic conductivity and thermo-chemical stability [6, 7].

EXPERIMENTAL

The materials are synthesized using sol-gel method, with citric acid and aquadest as chelating agents. For synthesizing $La_{1-x}Sr_xFeO_3$ (x = 0.1-0.4), each 30 mmol of corresponding composition of La_2O_3, $Sr(NO_3)_2$, and $Fe(NO_3)_3.9H_2O$ were mixed with the chelating agents in a beaker glass. Then, each colloid phase sample was heated and stirred on a Magnetic stirrer – Hot plate (WiseStir MSH-20D), with temperature of 120 °C and rotational speed of 700 rpm. After each sample transforms into the gel phase, it experienced gradual heat treatments (200 °C for 5 h, 900 °C for 6 h). Finally, the resulting powder was pressed into pellet with pressure of 5 ton/ square inch for 120 s and then sintered at 1300 °C for 1 h.

The XRD characterizations of the sintered pellets were done at room temperature, by Rigaku MiniFlex 600 X-Ray Diffractometer with radiation source of Cu Kα (λ = 1.5418 Å), with the 2θ range from 20° to 90°. The topography of all samples was investigated by SEM, using JEOL JSM-6510 LA electron microscope with acceleration voltage of 20 kV and magnification of 50000 ×. For the IS characterization, each pellet was modeled as parallel plate capacitor, connected with probe, and then connected to a Fluke PM6306 RLC meter. As function of frequency, the frequencies used are 1 MHz, 100 kHz, 10 kHz, and 1 kHz.

RESULTS AND DISCUSSION

Table 1 lists the measured structure identities of all $La_{1-x}Sr_xFeO_3$ sintered pellets. The grain sizes were calculated using Scherrer equation (Equation 4) [8], and the tolerance factors follow Goldschmidt equation (Equation 5) [5].

$$\tau = \frac{K\lambda}{B\cos\theta} \tag{4}$$

On Equation 4, K is the shape factor usually values 0.9, λ is the used X-ray wavelength, B is the Full Width at Half Maximum (FWHM) of the selected peak on radian, and θ is the Bragg angle. As an approach, Scherrer equation may give different crystallite size value, compared with the electron microscope characterization, if the tested crystal experienced inhomogeneous strain and crystal defect.

$$t = \frac{r_A + r_O}{2^{1/2}(r_B + r_O)} \tag{5}$$

On Equation 5, r_A, r_B, r_O are the ionic radius of A-site cation, B-site cation, and Oxygen anion, respectively. The less the tolerance factor value from unity, the lower the crystal structure regularity level of the perovskite [9].

The table of structure identities indicates that lattice parameters are changing, due to Sr and La concentrations difference on the $La_{1-x}Sr_xFeO_3$ samples. It is shown that the (a) lattice parameter and density tend to decrease with the increase of Sr doping, although all samples had the orthorhombic structure. The obtainable grain sizes of each sample also tend to decrease with the increase of Sr doping. This phenomenon shows that Sr doping on $LaFeO_3$ would cause an oxidation of Fe element on B-site, from Fe^{3+} to Fe^{4+} with smaller ionic radius, in order to balance the total charge [6].

Table 2 lists the unit cell positions and oxidation numbers of the 5 measured elements on XRD characterization of the samples. The table of the position of measured elements, show that the atomic position on the crystalline unit cell of all samples (with Fe atom as the owner of (0,0,0) coordinate) has been able to retain its stability along with Sr doping increase. The atomic position that has reached stable condition along with A-site element composition alteration, implying that the difference only happens on the ratio of Sr and La elements. Goldschmidt tolerance factor of all samples, support the fact that the cation order increase (value approaching 1 from below) along with the Sr doping increase [5].

TABLE 1. Structure identities of $La_{1-x}Sr_xFeO_3$ sintered pellets.

Identity	x = 0.1	x = 0.2	x = 0.3	x = 0.4
Crystal Structure	Orthorhombic	Orthorhombic	Orthorhombic	Orthorhombic
Space grup	Pnma	Pnma	Pnma	Pnma
a (Å)	5.560	5.555	5.555	5.532
b (Å)	7.842	7.855	7.805	7.810
c (Å)	5.537	5.514	5.524	5.487
Grain size (nm)	36	23	22	21
Density (gr/cm^3)	6.54	6.42	6.30	6.23
Tolerance factor	0.887	0.893	0.898	0.903

TABLE 2. Unit cell position of the related elements of $La_{1-x}Sr_xFeO_3$ sintered pellets.

Element	Sr	La	Fe	O1	O2
x^a	0.4720	0.4720	0.0000	0.2130	0.5120
x^b	0.4724	0.4724	0.0000	0.2290	0.5060
y^a	0.2500	0.2500	0.0000	0.0350	0.2500
y^b	0.2500	0.2500	0.0000	0.0350	0.2500
z^a	0.0070	0.0070	0.0000	0.2840	0.5660
z^b	0.0010	0.0010	0.0000	0.2660	0.5700
Oxidation numbers	+2	+3	+3	-2	-2

[a] Position of x = 0.1 sample.
[b] Position of x = 0.2, 0.3, 0.4 samples.

Figure 1 shows the atomic position manifestations on the $La_{1-x}Sr_xFeO_3$ lattice. The manifestations show that there is a uniformity of crystal structure of all samples (Orthorhombic), and significant difference happens only on the ratio of Sr and La elements.

Figure 2 shows the SEM images of $La_{1-x}Sr_xFeO_3$ samples. SEM images show that the grain distribution of the samples is uniform and good enough, with some grain agglomeration observed. There are no obvious signs of secondary phases observed on the images. Moreover, the display of the grain sizes tends to decrease along with Sr doping increase, supporting the previous results. To measure or indicate further about the grain uniformity, it is possible to use scientific image processing software on the sample figures in the future.

Using the measuring bar included in the SEM images of the samples, $La_{0.9}Sr_{0.1}FeO_3$ sample had the agglomeration size of about 0.5 μm. With the same method, $La_{0.7}Sr_{0.3}FeO_3$ sample had the grain size of about 0.133 μm, with agglomeration size of about 0.5 μm. This agglomeration condition makes it rather hard to distinguish between the grain and the grain boundaries, indicating that the contribution of the grain boundary in measured impedance would show inhomogeneous values, compared with the grain contribution.

Figure 3 shows the Nyquist plots of all $La_{1-x}Sr_xFeO_3$ samples on RT. The RT Nyquist plots show the tendency of the plot radius to decrease (hence impedance decrease) along with increasing Sr doping. This phenomenon implying that the oxygen vacancy δ which become charge carrier conductivity path in the samples is increasing along with Sr doping increase [3]. Therefore, ionic conductivity (Equation 2) in the samples had bigger influence compared with electronic conductivity (Equation 1) for total electrical conductivity, causing more conductivity with more dopant.

The double semicircle Nyquist plots are fitted using ZSimpWin software, that aims to acquire the appropriate equivalent electronic circuits and the component values. The proposed equivalent electronic circuit as the electrical properties model is the (RC)(RC) circuit, where one (RC) part represents grain contribution and the another (RC) part represents grain boundary contribution.

Using ZSimpWin software and the Nyquist plots, the component values of this equivalent electronic circuit have been obtained for each composition, written in Table 3. It can be concluded that the multiplication of R and C (also known as relaxation time τ) from grain contribution is having tendency to be smaller than the ones from grain boundary contributions. That means for the process of conduction in $La_{1-x}Sr_xFeO_3$, grain conduction is more reliable than the grain boundary conduction, probably due to agglomeration observed that blur the grain boundaries [10].

Figure 4 shows the Bode plots of the $La_{1-x}Sr_xFeO_3$ samples on RT. The Bode plots show that the curve shape of the real impedances Z' is more like the total impedances Z, compared with the curve shape of the imaginary

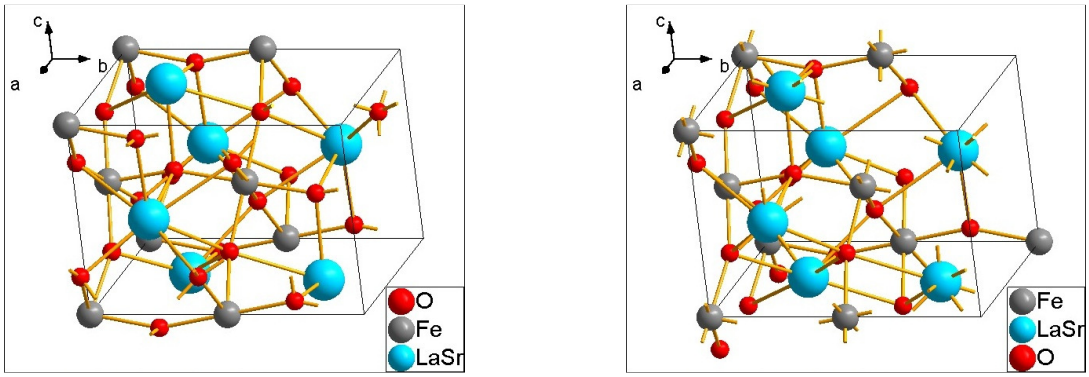

(a) (b)

FIGURE 1. Atomic position on $La_{1-x}Sr_xFeO_3$ lattice, with (a) x = 0.1, (b) x = 0.2, 0.3, 0.4. For the latter samples, the a and c lattice parameters are tend to decrease with x increase.

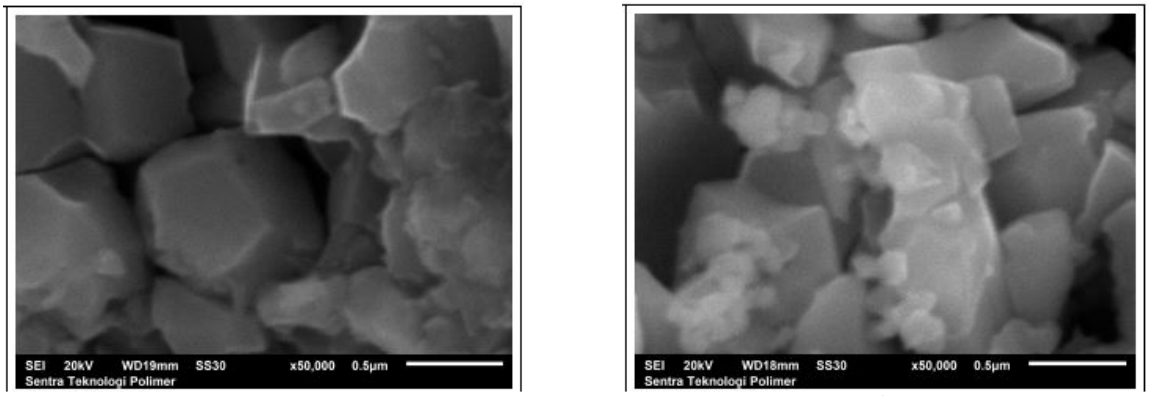

(a) (b)

FIGURE 2. 50000 × magnification SEM images of $La_{1-x}Sr_xFeO_3$, with (a) x = 0.1, (b) x = 0.3.

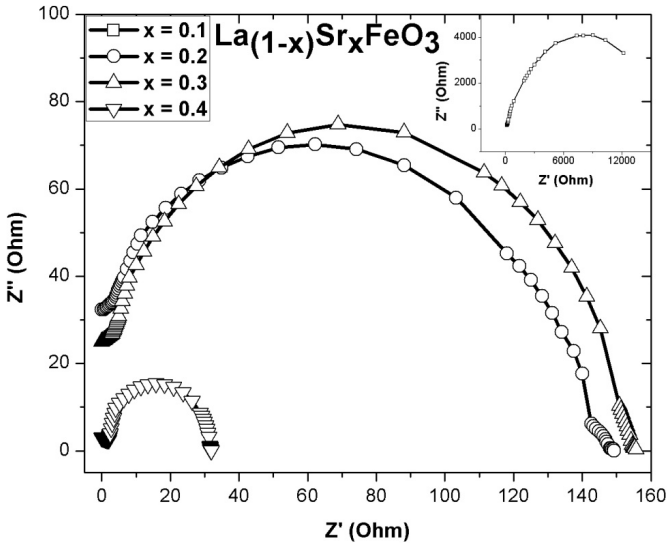

FIGURE 3. Nyquist plots of the $La_{1-x}Sr_xFeO_3$ samples on RT, with inset showing x = 0.1 plot in particular.

TABLE 3. Electrical properties modeling component values of $La_{1-x}Sr_xFeO_3$ at RT.

Sample	R1 (Ω)	C1 (F)	R2 (Ω)	C2 (F)
x = 0.1	281.10	5.151×10^{-07}	903.50	3.669×10^{-03}
x = 0.2	148.30	4.424×10^{-06}	1.97	4.322×10^{-20}
x = 0.3	15.40	5.841×10^{-06}	31.46	4.537×10^{-20}
x = 0.4	15.39	2.164×10^{-23}	29.28	2.669×10^{-05}

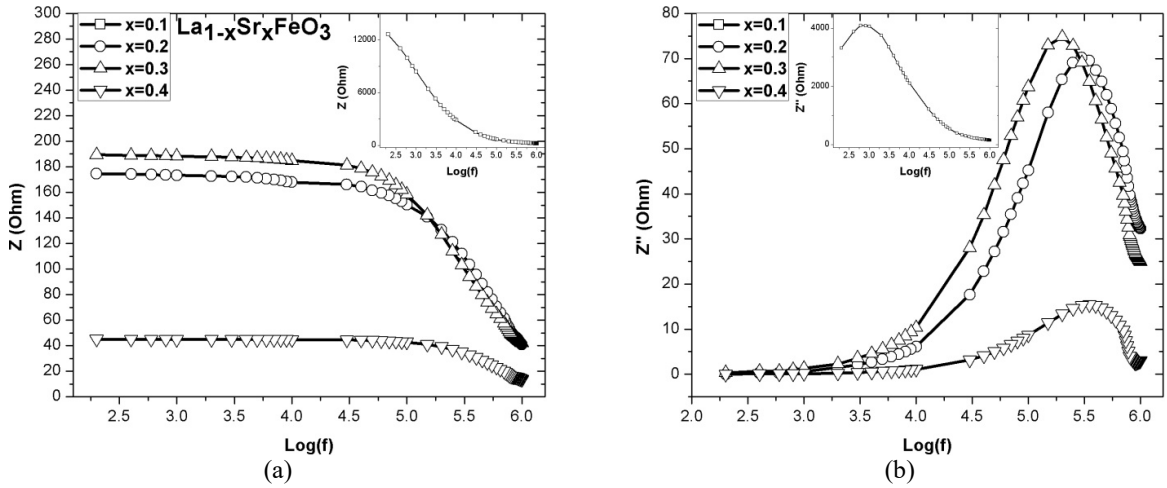

FIGURE 4. Bode plots of $La_{1-x}Sr_xFeO_3$ samples on RT, and inset showing x = 0.1 plot in particular, with the ordinate of (a) Z, (b) Z''.

impedances Z''. This resemblance means that the electrical conduction behavior of the sample is Resistive dominant, in accordance with complex impedance equation (Equation 6) [10].

$$Z = Z' + jZ'' = R + j\left(-\frac{1}{\omega C}\right) \tag{6}$$

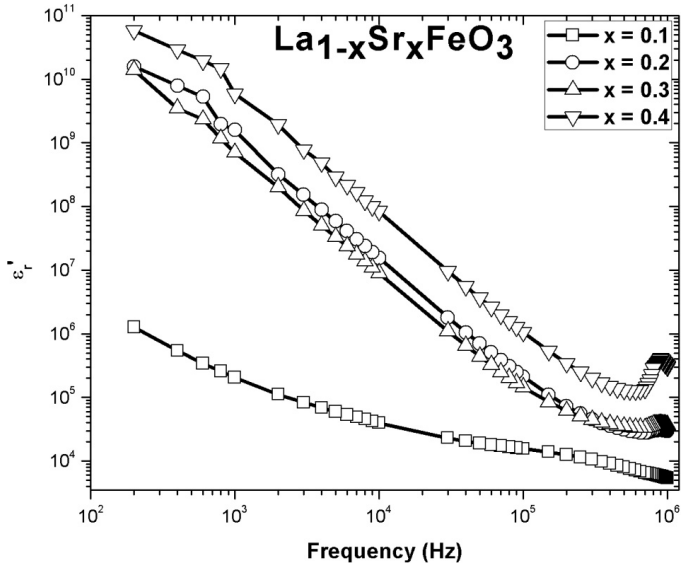

FIGURE 5. Real permittivity logarithmic plot versus frequencies for $La_{1-x}Sr_xFeO_3$ on RT.

Figure 5 shows $La_{1-x}Sr_xFeO_3$ real permittivity ε' curves toward frequencies on RT. The RT plot of real permittivity versus frequency shows that generally, the less the frequencies, the more the real permittivity values. For the x = 0.4 sample, it is observed that with frequency decrease, the real permittivity value decrease to a minimum point, and then increase to almost infinity. This phenomenon shows that on that composition, the Orthorhombic crystal structure is starting to be replaced with Rhombohedral crystal structure, causing differences on the electrical properties [6]. The stable, ideal values of real permittivity are obtained for both $La_{0.8}Sr_{0.2}FeO_3$ and $La_{0.7}Sr_{0.3}FeO_3$. Because both real and imaginary permittivities are inversely proportional to frequency, there is an assumption that the imaginary permittivity also follows the same trend [10].

CONCLUSIONS

$La_{1-x}Sr_xFeO_3$ (x = 0.1-0.4) were successfully synthesized by sol-gel method. XRD results show single phase Orthorhombic Perovskite crystal structure with Pnma space group. SEM images show that the samples are uniform and quite good in grain distribution, with a few grain agglomeration observed. The increasing Sr dopant composition on $LaFeO_3$ cause decreasing lattice parameters and grain sizes, due to oxidation of Fe from Fe^{3+} to Fe^{4+}. Moreover, the same increase also causes the crystal structure of the samples getting closer to regularity.

Impedance Spectroscopy characterization shows that the measured impedance tends to decrease along with Sr doping increase, implying that the oxygen vacancy δ that acted as charge carrier conductivity path is increasing. The ionic conductivity had more influence that the electronic conductivity, because the measured Fe cation still had the oxidation number of +3 for all the $La_{1-x}Sr_xFeO_3$ samples, yet we are able to predict that the same samples had experienced oxygen vacancy δ. The test to obtain an accurate result of δ for each sample as a function of temperature (for example, using thermo-analyzer in a reduction atmosphere) may be proposed in the future.

The electrical conductivity of $La_{1-x}Sr_xFeO_3$ is contributed by both grain and grain boundary. Bode plots with Z ordinate show the shift of highpoints with composition increase, and ones with Z' ordinate show that the main electrical conduction behavior is Resistive. Room temperature electrical permittivity behavior curves show that both $La_{0.8}Sr_{0.2}FeO_3$ and $La_{0.7}Sr_{0.3}FeO_3$ have the similar results, that although are not the largest, their values are stable.

REFERENCES

1. S. Phokha, S. Pinitsoontorn, S. Rujirawat, and S. Maensiri, Physica B Condens. Matter **476**, 55–60 (2015).
2. A. Benali, S. Azizi, M. Bejar, E. Dhahri, and M. F. P. Graça, Ceram. Int. **40**, 14367–14373 (2014).
3. F. He *et al*., Fuel **108**, 465–473 (2013).
4. K. Fan, H. Qin, L. Wang, L. Ju, and J. Hu, Sens. Actuators B Chem. **177**, 265–269 (2013).
5. O. Clemens, M. Kuhn, and R. Haberkorn, J. Solid State Chem. **184**, 2870–2876 (2011).
6. X. Cui, S. Li, and X. Zhu, Mat. Lett. **130**, 267–270 (2014).
7. M. Kuhn, S. Hashimoto, K. Sato, K. Yashiro, and J. Mizusaki, Solid State Ionics **195**, 7–15 (2011).
8. B. D. Cullity, *Elements of X-ray Diffraction, 2nd Edition* (Addison-Wesley, Boston, 1978).
9. H. B. Khlifa *et al.*, J. Alloys Compd. **680**, 388-396 (2016).
10. J. R. Macdonald, *Impedance Spectroscopy: Theory, Experiment, and Applications, 2nd Edition*, edited by E. Barsoukov (John Wiley & Sons, Hoboken, New Jersey, 2005).